International Journal of Hydrogen Energy 89 (2024) 977–989

Contents lists available at ScienceDirect

International Journal of Hydrogen Energy

journal homepage: www.elsevier.com/locate/he

Enhancing hydrogen evolution: Carbon nanotubes as a scaffold for Mo_2C deposition via magnetron sputtering and chemical vapor deposition

Shubhadeep Majumdar [a,b,*], Stefanos Chaitoglou [a,b,**], Jarosław Serafin [a,c], Ghulam Farid [a,b], Rogelio Ospina [a,b,d], Yang Ma [a,b], Roger Amade Rovira [a,b], Enric Bertran-Serra [a,b]

[a] Department of Applied Physics, University of Barcelona, C/Martí i Franquès, 1, 08028, Barcelona, Catalunya, Spain
[b] ENPHOCAMAT Group, Institute of Nanoscience and Nanotechnology (IN2UB), University of Barcelona, C/ Martí i Franquès, 1, 08028, Barcelona, Catalunya, Spain
[c] Department of Inorganic and Organic Chemistry, University of Barcelona, C/Martí i Franquès, 1, 08028, Barcelona, Catalunya, Spain
[d] Escuela de Física, Universidad Industrial de Santander, Carrera 27 Calle 9 Ciudad Universitaria, Bucaramanga, Colombia

ARTICLE INFO

Handling Editor: Suleyman I. Allakhverdiev

Keywords:
Carbon nanotubes
RF magnetron sputtering
Chemical vapor deposition
Mo_2C
HER
Green hydrogen

ABSTRACT

This study presents an innovative approach to fabricating carbon nanotubes (CNTs) through magnetron sputtering and chemical vapor deposition (CVD). These CNTs serve as a robust structural scaffold for the deposition of molybdenum, which, through thermal annealing, becomes molybdenum carbide (Mo_2C), which is highly efficient for hydrogen evolution reaction (HER). Our investigation delves into the physical and chemical attributes of these electrodes, revealing insights into the functionality of Mo_2C on CNTs hybrid structures. Chemical characterization confirms the exceptional performance of the electrode. Our Mo_2C on CNT hybrid system showcases remarkable electrocatalytic activity, with an onset potential of 103 mV at 1 mA/cm^2 and an overpotential of 176 mV at 10 mA/cm^2. Further validation comes from tests revealing a Tafel slope of 95 mV/dec, affirming its superiority in facilitating HER. Unparalleled combination of low charge transfer resistance and accelerated reaction kinetics, Mo_2C on CNTs hybrid structure is poised to significantly enhance HER activity.

1. Introduction

As the demand for clean and sustainable energy solutions continues to surge, the scientific community has identified some key technologies that can make this shift happen smoothly. One of the most promising contenders to bring this change, is the extraction of clean hydrogen by electrochemical decomposition of water [1,2]. Hydrogen has a high energy density, and can be efficiently stored and converted into energy, on demand [3,4].

The electrochemical splitting of water is a carbon neutral process, and produces no harmful by-products [5,6]. The efficiency of this process depends on the electrocatalyst used, which, unfortunately, is achieved with very expensive and scarce metals such as platinum, palladium, gold, rhodium, ruthenium, as most prominent. Generally, noble metals such as platinum and palladium set the standards for some of the most efficient electrode materials [7–9], but given their scarcity and cost, they are not feasible when it comes to actual practicality, and therefore this work focuses on finding a more feasible electrode whose working efficiency can be comparable to these ideal reference electrodes.

The challenge to make this process ubiquitous is finding an excellent electrocatalyst material which is abundant, cheap and can be mass manufactured [10]. Transition metal (TM) compounds are being extensively studied for this application and show a huge potential for use in HER [11–14]. Transition metal carbides (TMCs), particularly Mo_2C, have demonstrated electrocatalytic activities that approach those of noble metals [15–21]. The interstitial incorporation of carbon within the metal lattice of Mo_2C leads to an increased metal–metal bond distance and a higher density of states near the Fermi level, resulting in unique surface reactivity [16]. Experimental evidence supports the efficacy of Mo_2C as a promising catalyst for hydrogen evolution reactions (HER) in acidic environments [22–24].

To get the most out of the electrocatalytic effects of Mo_2C we need to expose a large surface area of the material to the electrolyte [25]. Nanoparticles have a much higher surface area compared to bulk metal; therefore, we deposit nanoparticles of molybdenum on a suitable

* Corresponding author. Department of Applied Physics, University of Barcelona, C/Martí i Franquès, 1, 08028, Barcelona, Catalunya, Spain.
** Corresponding author. Department of Applied Physics, University of Barcelona, C/Martí i Franquès, 1, 08028, Barcelona, Catalunya, Spain.
E-mail addresses: shmajumm110@alumnes.ub.edu (S. Majumdar), stefanoschaitoglou@ub.edu (S. Chaitoglou).

https://doi.org/10.1016/j.ijhydene.2024.09.425
Received 5 July 2024; Received in revised form 27 September 2024; Accepted 29 September 2024
Available online 2 October 2024

scaffold to maximize the active sites [26]. Carbon nano structures (CNS) are ideal to be used as scaffolds, as they are chemically stable in acidic and alkaline electrolytes, conductive to electricity, mechanically strong and generally boast a large surface area. The ease of functionalizing these CNS also makes them a lucrative choice for supporting structures to be used in electrodes.

The choice of supporting structure for this study was CNTs grown on a graphite felt substrate, provided that graphite felts are an excellent choice for three dimensional electrodes [27,28]. The graphite felt has a porous structure with a large number of individual carbon fibers [29]. This comes with suitable advantages for our purpose, firstly the high conductivity of carbon fibers guarantees a low series resistance, secondly the high porosity of the substrate allows the electrolyte solution to disperse itself, which gives a larger surface area for reaction, thirdly the individual carbon fibers have CNTs grown on them, which further increases the surface area of reaction, and gives another boost to the active sites on the electrode, and lastly both CNTs and the graphite felts are highly stable in acidic conditions, which makes this a highly enduring material when exposed to the acidic electrolyte and ensures long term electrode stability [30,31]. The use of CNTs and the carbon fibers on which they are grown, also help in the increase of conductivity of the Mo_2C particles [32].

This study therefore focuses on leveraging the electrocatalytic performance of Mo_2C by depositing it on a suitable architecture like CNTs grown on graphitic felt. Moreover, we provide insights on the dual role of CNTs, as both a growth template for the Mo compounds, as well as a C precursor during the carburization step. We argue that loosely-bonded C species migrate towards Mo and react with it, a mechanism that has been reported before for the case of Mo carburization on graphene templates [14] (Scheme 1). To test the capabilities and to have a point of reference for the performance of the Mo_2C on CNTs hybrid, we also use a Mo on CNTs electrode to undergo the same tests, to verify how much of a difference in HER performance is obtained by the carburization of molybdenum.

2. Materials and methods

2.1. Preparation of the nano structured electrodes

The CNTs are grown using a CVD process with acetylene on a catalytic system consisting of thin film layers of aluminum and iron, which are previously deposited on graphite felt by magnetron sputtering. The CNTs are then functionalized by molybdenum using magnetron sputtering and then carburized in an inert Ar environment by annealing at high temperatures, leading to the in-situ carburization of the molybdenum into molybdenum carbide. The morphology of these Mo_2C on CNTs hybrid is then studied using SEM and TEM imaging and more detailed physical characterization is obtained by using XRD, XPS and Raman Spectroscopy. The chemical characterization is done using linear sweep voltammetry, electrochemical impedance spectroscopy and chronoamperometry.

2.1.1. Sputtering of the seed layer for the growth of carbon nanotubes

The CNTs are grown on a graphite felt substrate (from MERSEN IBERICA). The dimensions of the graphite felt substrate used are approximately 5.5 cm × 3.5 cm. The substrate is placed in the sputtering reactor and when a base pressure of approximately $5x10^{-4}$ Pa is reached, the sputtering chamber is filled by argon. A 10 nm aluminum nanofilm is then deposited, followed by a 3 nm iron nanofilm, both using magnetron sputtering with 99.99% pure aluminum and iron targets. The plasma is created using argon at 1 Pa and 100 W of DC-pulsed power (100 kHz pulses and 10% of positive duty cycle) for the deposition of 10 nm of aluminum, taking 46 s, and argon at 2 Pa and 50 W of DC-pulsed power for the deposition of 3 nm of iron, taking 30 s. All depositions are conducted at room temperature.

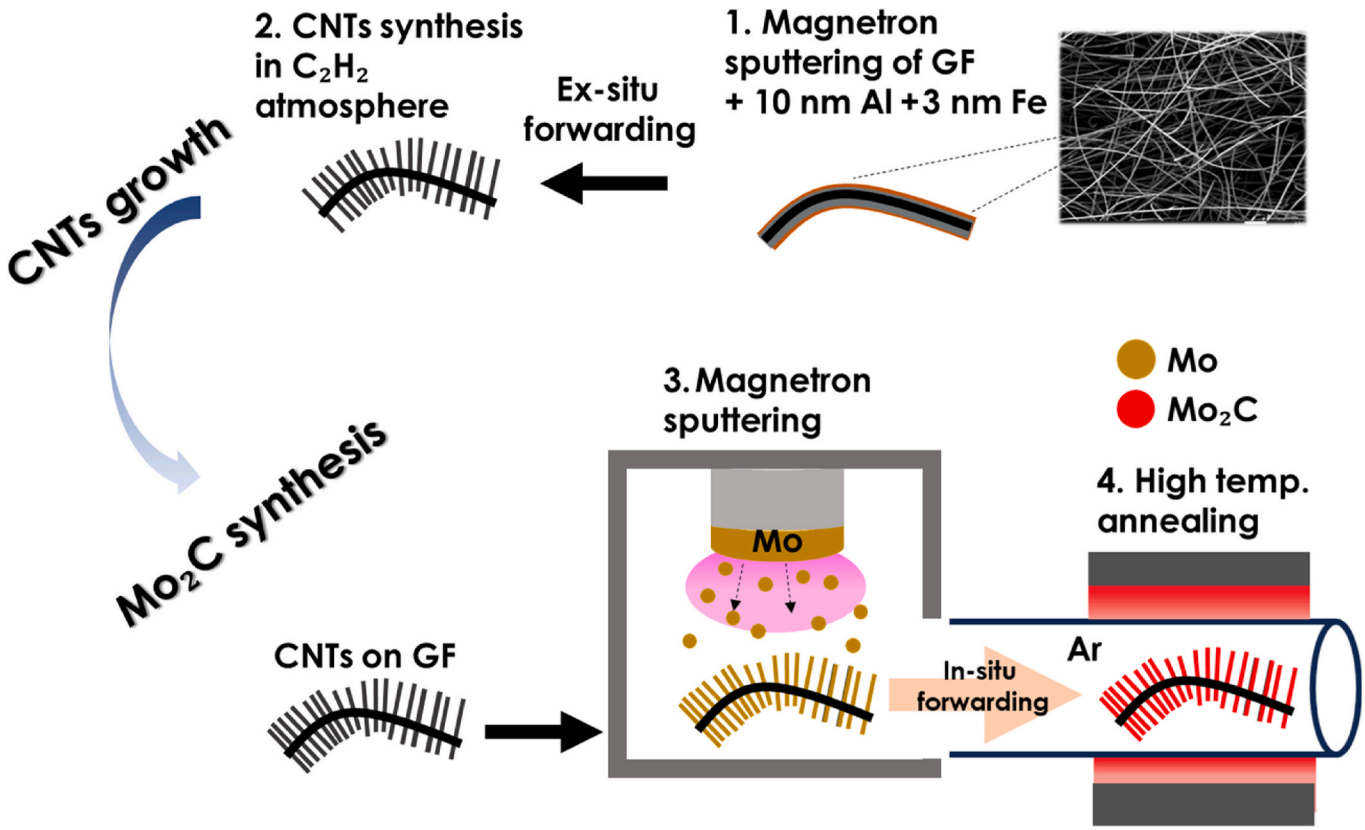

Scheme 1. Graphical representation of the fabrication of Mo_2C on CNTs hybrid structure.

2.1.2. Growth of carbon nanotubes on graphite felt substrate

The aluminum and iron-coated sample is then placed in a quartz tube reactor, and a chemical vapor deposition (CVD) process is employed for the growth of carbon nanotubes. The sample is heated to a temperature of 800 °C at atmospheric pressure and allowed to thermalize at this temperature for 15 min in an environment of argon and hydrogen, with respective flow rates of 14 sccm and 100 sccm. After the thermalization period, acetylene is introduced into the chamber at a flow rate of 5.8 sccm. This process involves water-assisted growth, necessitating the introduction of a low flow of argon through a Dreschel bottle containing water which supplies a low amount of argon mixed with water vapours to enable water-assisted growth of carbon nanotubes on individual carbon fibers of the graphite felt substrate. The flow of acetylene is maintained for 5 min, after which both the acetylene and hydrogen flows are shut down. The flow from the Dreschel bottle is then allowed to continue to flow for another 5 min, after which the heater is turned off, followed by the cessation of the water-assisted argon gas flow. Only pure argon is permitted to flow in the chamber as the sample's temperature gradually decreases from 800 °C to approximately 50 °C, at which point the sample is removed from the reactor.

2.1.3. Deposition of molybdenum on the carbon nanotube, followed by carburization of the molybdenum

The grown carbon nanotubes are subsequently transferred to another reactor capable of depositing molybdenum by magnetron sputtering, followed by a quartz heating tube used for annealing to carry out an in-situ carburization of the molybdenum avoiding the risk of oxidization of the freshly deposited molybdenum layer. The sputtering chamber and the quartz tube are interconnected, enabling the transfer of the sample between the two chambers under vacuum conditions. After reaching a base pressure close to 10^{-4} Pa, molybdenum is sputtered at room temperature, using an RF power (13.56 MHz) of 100W in the presence of 1 Pa of argon in the chamber. The magnetron sputtering is done for 10 min at a 1 nm/min deposition rate. Following the completion of the deposition, the carbon nanotubes with molybdenum deposition are introduced into the quartz heating tube, where the sample undergoes annealing for 5 min at a temperature of 960 °C in an inert argon environment where the pressure is maintained at 1Pa with an Ar flow of 10 sccm, resulting in successful in-situ carburization and the formation of carbon nanotubes functionalized by molybdenum carbide. The carburization process is confirmed through the XRD and Raman Spectroscopy results, which will be discussed in detail later. For this study, two samples were fabricated: one with molybdenum deposition on carbon nanotubes (Mo on CNTs), and the with molybdenum deposition followed by further carburized in an argon environment, leading to the formation of molybdenum carbide on carbon nanotubes (Mo_2C on CNTs).

2.2. Surface analysis

The surface analysis of the samples was conducted using scanning and transmission electronic microscopy (SEM and TEM), X-ray diffraction (XRD), X-ray photoelectron spectroscopy (XPS), and Raman spectroscopy. SEM was used to investigate the morphology of the molybdenum carbide on carbon nanotubes, with the sample cut into approximately 1 cm × 1 cm square for observation. exploration was made using the FESEM JEOL JSM-7001F at 15 kV and the SEM JEOL J-6510 at 10 KV. TEM imaging was performed using JEOL 1010 at 200 kV. Sample preparation involved brushing the surface of the sample containing molybdenum carbide and carbon nanotubes with a cotton swap, dispersing it in ethanol, drop-casting it on a Cu grid, and allowing it to dry, leaving behind the structures for analysis. ImageJ and Digital Micrograph were used to analyse the SEM and TEM images. ImageJ software was used for the statistical analysis of the TEM Images. XRD analysis was carried out using the Anton Paar XRDynamic 500 multipurpose powder diffractometer in Bragg-Brentano mode with a 360 mm radius. The sample was exposed to Cu $K\alpha_{(1+2)}$ radiation with a wavelength of 1.5418 Å, and $2\theta/\theta$ scans were conducted from 4° to 100°, with 2θ step size of 0.02° and each measurement step lasting 30s. XPS analysis was performed with the PHI 5500 Multi-Technique System (from Physical Electronics, Chanhassen, MN, USA) using a monochromatic X-Ray source (Al Kα line of 1486.6eV and 350W. The area analysed had a diameter of 0.8 mm, with Survey XPS spectra having a pass energy of 187.5eV and 0.8eV/step, and elemental spectra having a pass energy of 11.75eV and 0.1eV/step. Raman spectroscopy was employed to further study the molybdenum carbide on carbon nanotubes revealing the vibrational modes. The Raman microscope used was HR800, Lab-Ram (HORIBA France SAS, Palaiseau, France), equipped with a 532 nm solid-state laser, operating at a power of 5 mW with an irradiation area diameter of 1 μm.

2.3. Electrochemical characterization

The electrochemical behaviour of the sample was investigated for hydrogen evolution reaction (HER) using a potentiostat/galvanostat (AutoLab, PGSTAT30, Eco Chemie B.V.). The experiments were conducted using a 3-electrode system at room temperature. An Ag/AgCl electrode with an internal 3 M KCl solution served as the reference electrode, while a Pt electrode (Metrohm) was utilized as the counter electrodes. The samples under study constituted the working electrode, which was connected to the power supply using a graphite rod and a crocodile clip. The sample was cut to achieve a surface area of 1 cm^2.

Linear sweep voltammetry was performed with a scan rate of 5 mVs^{-1} using a 1 M H_2SO_4 electrolyte. Chronoamperometry tests were performed to assess the electrode endurance, using a constant bias of 410 mV. The charge transfer resistance was evaluated via electrochemical impedance spectroscopy (EIS) across a frequency range from 100 kHz to 1Hz. CV scans were performed to find the double layer capacitance and the electrochemical active surface area (ECSA) of 4 samples (Graphite felt, CNTs, Mo on CNTs and Mo_2C on CNTs). The CV scan graphs were further smoothed using adjacent averaging method on Origin.

3. Results and discussions

3.1. Synthesis and characterization of nanostructured Mo_2C on CNTs

CNTs were grown on a graphite felt substrate and were functionalized with molybdenum. One sample retained molybdenum sputtered on CNTs, while the other underwent further carburization to improve its performance for HER. Graphite felt substrates possess desirable properties for HER, including a large surface area, high porosity and mechanical and chemical stability. Fig. 1a and b depict the graphite felt substrate with grown CNTs, functionalized with Mo_2C. The images reveal the dense network of individual carbon fibers, constituting the scaffold for the Mo_2C on CNTs structures. Fig. 1a demonstrates CNT growth not only on the surface layer of the felt but also on deeper layers, while Fig. 1b shows a magnified image of a single carbon fiber, revealing two distinct structures of CNTs. One group exhibits shorter, less dense CNTs in the fiber's center, while the other displays longer, denser and more ordered CNTs curling along the fiber's periphery, providing a continuous surface. Fig. 1d illustrates the differing morphologies of molybdenum particles deposited on the CNT surfaces. The particles are homogeneously deposited on the surface of both curly and randomly oriented CNTs. The EDS elemental map in Fig. 1d confirms the homogeneous deposition of Mo particles on CNTs. EDS analysis in Fig. 1c, conclusively confirms the successful functionalization of the CNTs with molybdenum. Carbon signal at 0.27 KeV is noted, originating from both the CNTs and the substrate itself, along with the detection of iron at 0.95 KeV and 6.41 KeV and aluminium at 1.49 KeV attributed to the initial aluminium and iron layers deposited on the substrate for CNT growth and the signal for Mo is also noted at 2.3 KeV. There is also an additional

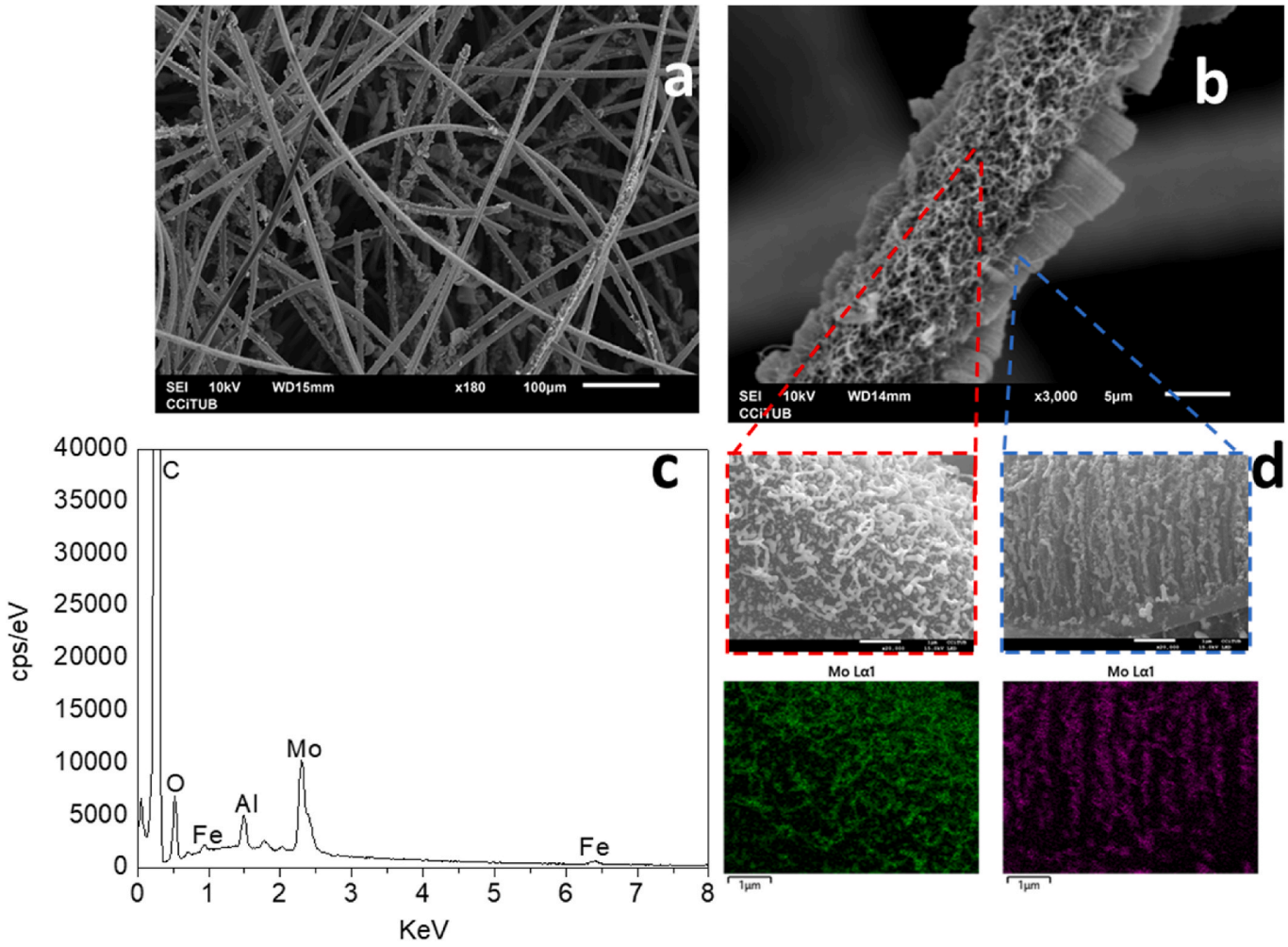

Fig. 1. SEM images of a) graphite felt substrate with CNTs grown on the individual carbon fiber b) single carbon fiber zoomed in to show the CNTs grown on the surface c) EDS spectra of the sample after deposition of molybdenum, showing the presence of carbon (from the substrate and CNTs), aluminum (from the seed layer) and molybdenum (from the functionalization of the CNTs) d) further zoom on the structure shown in b) which shows 2 distinct CNT structures, and the difference of the molybdenum deposition on these structures.

signal for oxygen at 0.52 KeV which is contributed by the ambient oxidation of Mo, Al and Fe when exposed to air.

In Fig. 2a, XRD results provide definitive evidence of molybdenum carburization. The diffraction peaks at 34.45°, 38.02° and 39.48° correspond to the (100), (002), (101) crystal planes of β-Mo_2C respectively [33], as confirmed by subsequent TEM imaging. Peaks observed in Fig. 2b at 25.5° and 42.6° represent characteristic peaks for graphitic structures, with the former attributed to the (002) plane and the latter attributing to the (100) plane which indicates the presence of turbostratic carbon structures, indicative of imperfect graphite crystals arranged in random directions. This turbostratic arrangement is common in carbon-based materials and underscores the intricate nature of the structural modifications induced by the carburization process [34]. The combination of XRD analysis and TEM imaging not only confirms the successful conversion of molybdenum to β-Mo_2C but also provides a comprehensive characterization of the co-existing graphitic carbon structures. This detailed structural insight is critical for understanding the material's enhanced catalytic properties and mechanical robustness imparted by the integration of β-Mo_2C nanoparticles onto the CNT surfaces [35].

The Raman spectra of both pristine Mo on CNTs (black spectrum) and Mo_2C on CNTs (red spectrum) are presented in Fig. 2c. Both spectra show Raman bands characteristic of graphitic carbon, specifically for multi-walled carbon nanotubes including peaks at 1345 cm^{-1} (D peak), 1583 cm^{-1} (G peak), and 2694 cm^{-1} (G' peak) [36]. These features provide conclusive evidence of in-situ molybdenum carburization, in an inert argon environment. The presence of Mo_2C peak at 139 cm^{-1} in the red-colored spectrum confirms carburization [37], indicating that the process occurred in-situ without the use of additional carbon precursor. Carburization involved annealing the molybdenum-coated sample at 960 °C for 5 min in an inert argon environment. It occurs through the migration of carbon atoms with free bonds, located on defective points on the carbon nanotubes, towards Mo particles and consecutive reaction [31].

In the black-colored spectrum, characteristic D, G and G' peaks of carbon corresponding to the CNTs present in the sample are evident. The D peak is associated with defects present in the graphitic structure of CNTs, while the G peak represents the graphitic structure itself. The absence of the A^1_{1g} peak characteristic of molybdenum carbide confirms the non-carburized state.

In the red-colored spectrum, a noticeable shift in the peaks D and G indicates a reduction in defects. The appearance of the A^1_{1g} peak provides evidence of molybdenum carbide presence, while recrystallization of leading to the reduction of the D peak [38]. Additionally, the reduction in the intensity of the D peak (I_D) relative to the G peak (I_G) suggests a decrease in the number of defects. This change in the I_D/I_G ratio signifies an improvement in the structural quality of the CNTs, with fewer disruptions in the graphitic lattice. These values provide a clear indication

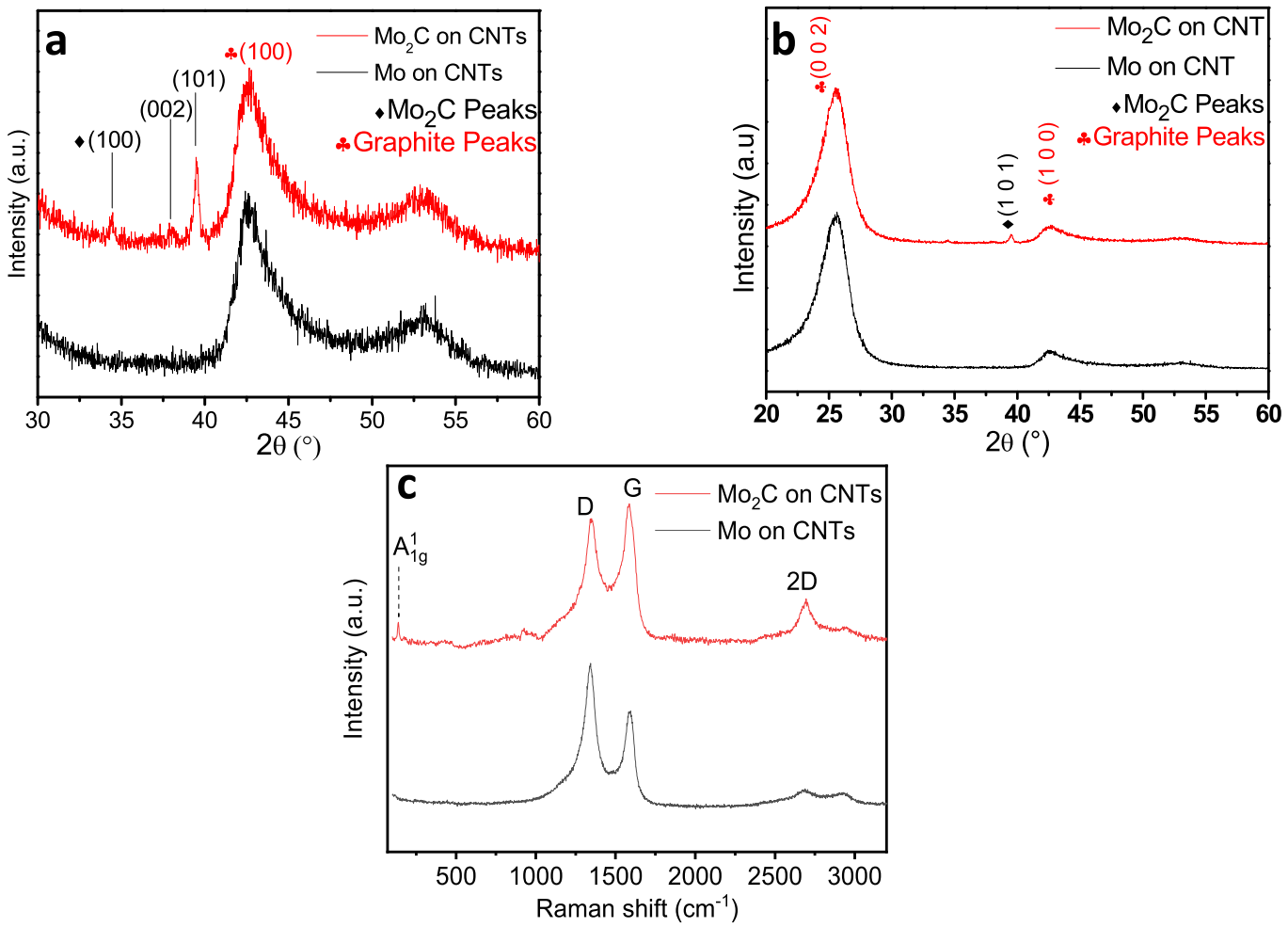

Fig. 2. a) XRD spectrum of Mo on CNT (in black) compared to Mo2C on CNT (in red) showing the Mo2C peaks b) Full XRD spectrum of Mo on CNT (in black) compared to Mo2C on CNT (in red) showing the graphite peaks c) Raman spectrum of Mo on CNT (in black) and Mo2C on CNT (in red). (For interpretation of the references to color in this figure legend, the reader is referred to the Web version of this article.)

of the changes in structural quality and defect density of the CNTs. The higher I_D/I_G ratio in the red spectrum (1.06) compared to the black spectrum (0.89) suggests a relative decrease in defects after carburization. Conversely, the I_G/I_D ratio in the red spectrum (0.94) being lower than that in the black spectrum (1.12) further supports the improved structural integrity of the CNTs post-carburization. The reduction of defects is important as it directly affects the electrocatalytic performance of the electrode. Defects in CNTs can trap charge carriers, reducing their mobility and impeding the HER. By minimizing defects, the mobility and availability of charge carriers increase, consequently enhancing electrocatalytic activity. This observation is supported by the electrochemical tests conducted and will be further discussed later.

TEM images in Fig. 3b and c depict Mo_2C molecules anchoring on a single CNT, with darker spots representing Mo_2C nanoparticles. A single multi-walled CNT serves as structural support for multiple Mo_2C nanoparticles, enhancing catalytic functionality by providing a large surface area for CNTs functionalization. Fig. 3a showcases a high-resolution TEM image of a single Mo_2C nanoparticle on a CNT. The anchoring of Mo_2C nanoparticles onto CNTs is crucial for several reasons. Firstly, the high surface area of CNTs provides ample sites for the attachment of Mo_2C nanoparticles, which is essential for maximizing catalytic activity. The Mo_2C nanoparticles are catalytically active towards various reactions, and their dispersion on the CNTs ensures that a large number of these active sites are available. Secondly, the intimate contact between the Mo_2C nanoparticles and the CNTs facilitates efficient electron transfer, which is vital for catalytic processes, especially in applications such as hydrogen evolution reactions or other electrochemical processes. Moreover, the size of the Mo_2C nanoparticles plays a critical role in their catalytic performance. Smaller nanoparticles typically have a higher surface-to-volume ratio, providing more active sites per unit volume compared to larger particles. The particle's size distribution histogram is depicted in Fig. 3d. Upon analysis of 89 individual Mo_2C nanoparticles, the average size was determined to be 4.7 nm with a standard deviation of 4.1 nm. The observed average size of 4.7 nm indicates that the nanoparticles are small enough to exploit this advantage, yet the standard deviation of 4.1 nm suggests there is a considerable range in particle sizes, which might influence the uniformity of catalytic activity across different nanoparticles. FFT analysis of the particles observed in Fig. 3a reveals characteristic lattice spacing of CNTs at 0.34 nm, consistent with the lattice spacing of graphitic carbon [39]. Additionally, a lattice spacing of 0.26 nm, indicative of Mo_2C presence, is observed [40]. This 0.26 nm lattice spacing corresponds to the crystal plane for Mo_2C_{100}, aligning with the data obtained by XRD and confirming successful Mo carburization.

The surface states were characterized using XPS. XPS analysis of three distinguish samples was performed. Pristine Mo deposited on CNTs, carburized Mo_2C on CNTs and Mo_2C on CNTs after the electrochemical endurance tests. The survey spectra in Fig. 4a reveal the presence of a strong signal from C, Mo and O which confirms the absence of contamination in the sample. Additionally, after electrochemical tests, it is observed that there is a small signal contributed by S, which is due to the formation of SO_2 (Sulphur dioxide) as a result of long-term

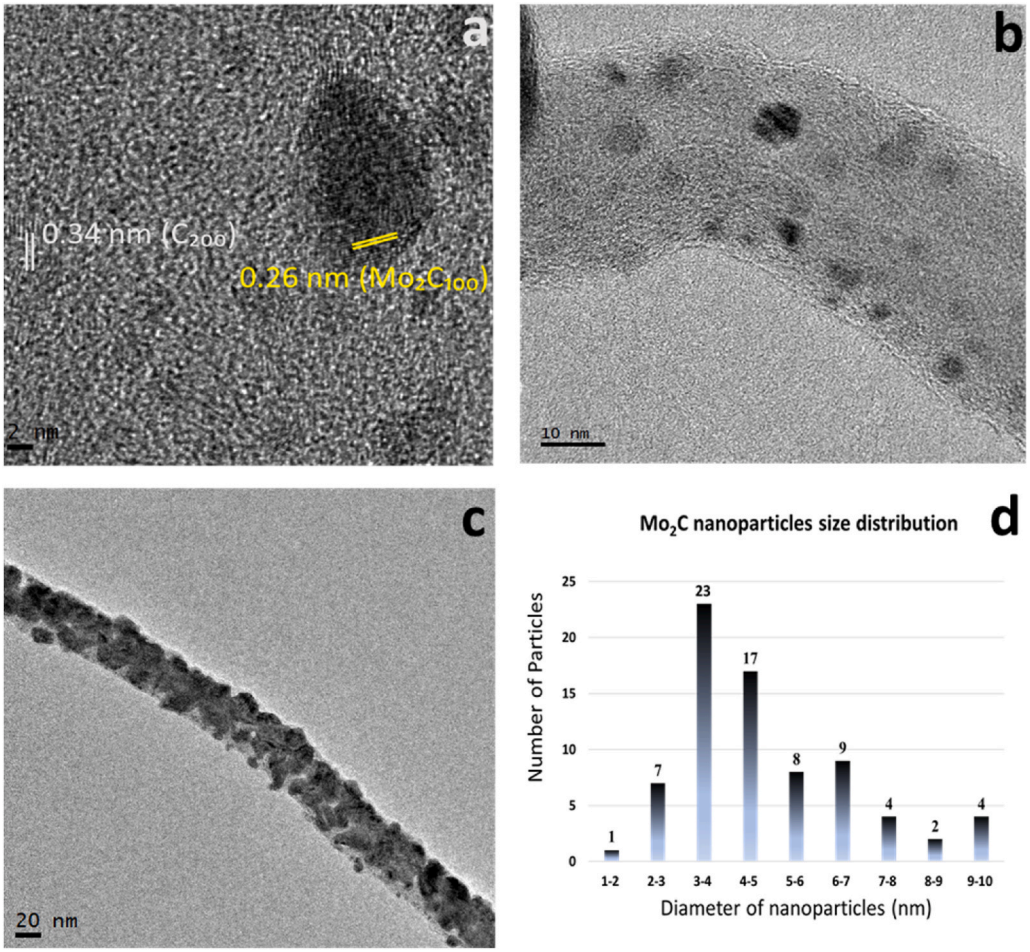

Fig. 3. TEM images of the Mo_2C on CNT sample, a) FFT analysis on the multiwalled CNT and Mo_2C particle to find their crystal planes, b) image of a single multiwalled CNT with multiple anchored Mo_2C nanoparticles on it, c) Image showing a single CNT with uniform Mo_2C deposition and d) Histogram showing the average molybdenum carbide nanoparticle diameter comparison using TEM imaging.

testing in a H_2SO_4 electrolyte. This is further supported by the reduction in the oxide peak observed in the Mo 3d spectra after electrochemical tests, implying the migration and reaction of oxygen molecules from Mo to S.

From the C 1s peaks in Fig. 4b we can identify the different compounds and molecular interactions happening in the samples and how various processes like annealing and interactions with acid changes and modifies the C and Mo structure and bonding. The main peak at 284 eV observed in all spectra is characteristic of the sp^2 configuration of the CNTs. CNT with Mo deposition reveals the C-related bonds in the sample by observing the peaks corresponding to C═O, C–O, C–C, C═C and C–Mo. The C═C contribution originates from the sp^2 configuration present on CNTs, while the most electropositive C–C contribution is related to the presence of defective carbon-carbon bonds. We can observe the same peaks in the spectra of CNT with Mo_2C which confirms that the annealing process does not affect or damage the structure and bonding of the CNTs, rather contributes to the carburization of the Mo. We see an interesting change in the C 1s spectra of the CNT with Mo_2C sample after electrochemical tests, when compared with the other two spectra. In this particular case there is an appearance of π- π* shake up satellites ranging from 287 to 290 eV [41]. This presence indicates that the interaction with acid has made the CNTs undergo structural reordering leading them to become more graphitic. This graphitization enhances the electrical conductivity of the material, which is beneficial for the HER as it makes the CNTs more chemically stable [42].

Mo 3d spectra for the 2 samples are shown in Fig. 4 c and d. In the sample with Mo on CNTs without annealing, the oxide peaks of MoO at 228.3 eV [43], MoO_2 at 229.3 eV [43] and MoO_3 at 232.4 eV [44] are shown. In the spectra of the Mo_2C on CNTs sample the peaks for MoO_2 at 229.3 eV and MoO_3 at 232.4 eV are observed. An additional Mo_2C-related peak arises at 227.9 eV and at 231 eV [16], proving the carburization upon annealing, in accordance with the XRD results. It is argued that oxidized Mo is present only in the surface of the Mo_2C particles, in the form of an ultrathin layer, which is electrochemically 'transparent' and therefore does not hinder the electrochemical activity of the core carbide particle. Further oxidation is limited due to the presence of an amorphous carbon layer coating the particle (Fig. S3), which suppress surface oxidation by acting as a mechanical barrier that blocks the volume expansion attributed to oxidation [37,45].Therefore, while a thin oxidized layer is present, its impact on the catalytic performance is negligible due to the protective role of the carbon coating.

3.2. *Electrochemical analysis for application in the electrocatalytic HER*

The fabricated samples underwent electrochemical tests to assess their electrocatalytic performance towards HER. The conducted tests included linear sweep voltammetry (LSV), electrochemical impedance spectroscopy (EIS), and chronoamperometry.

In Fig. 5a The LSV curve for a platinum electrode (green line), known for its superior HER performance albeit limited by scarcity and cost, serves as a reference for comparison with our samples. Pristine CNTs were not electrocatalytically active in the examined voltage window. The electrode's performances were compared with respect to onset and overpotential values required to generate 10 mA/cm^2, as solar light

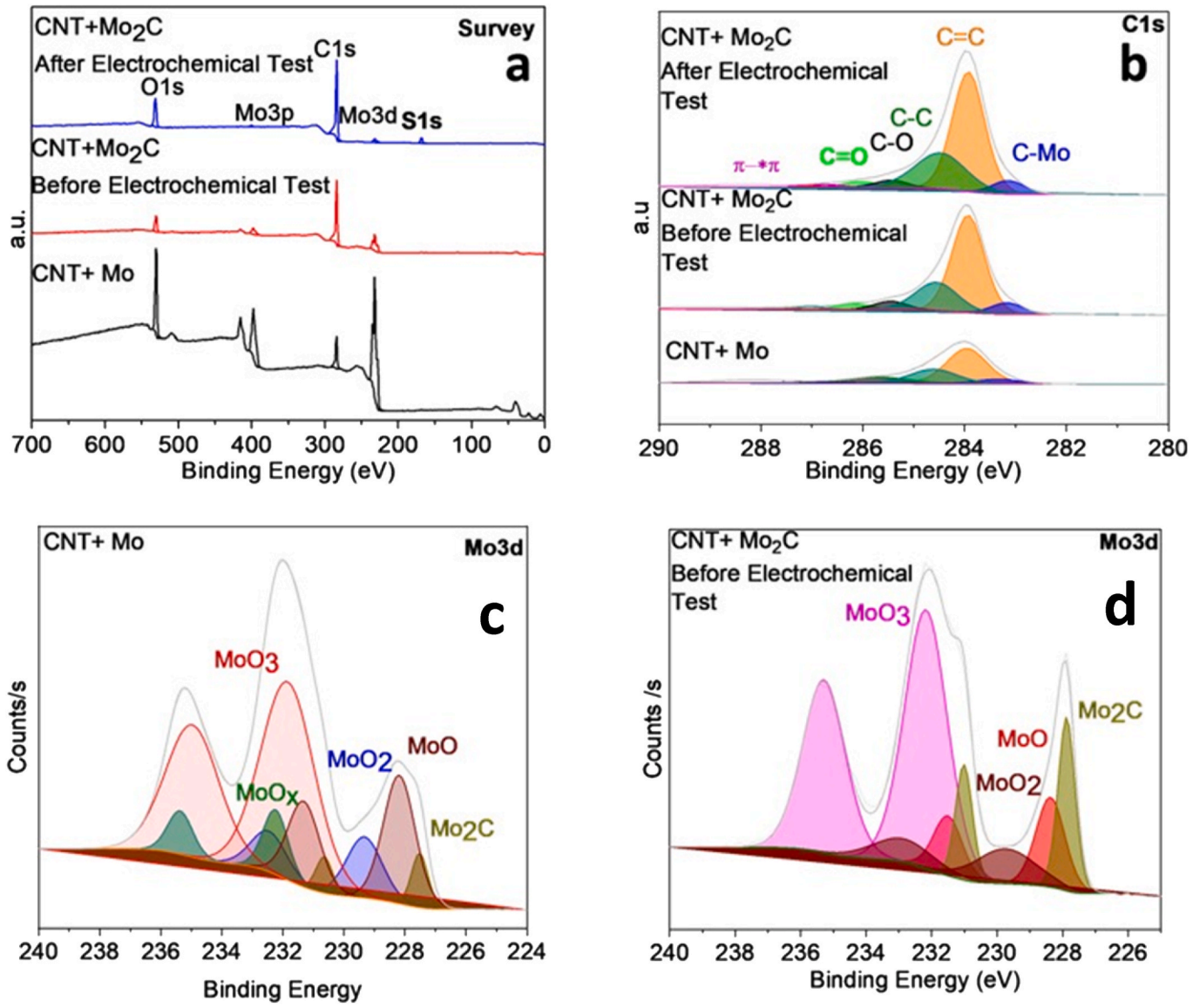

Fig. 4. XPS spectrum of the sample, namely a) survey spectra b) C 1s spectra c) Mo 3d of Mo on CNT sample d) Mo 3d of Mo_2C on CNT sample before electrochemical tests.

coupled HER processes generally take place at 10–20 mA/cm^2 under standard conditions and hence this serves as a practical reference point [46]. The as-sputtered Mo on CNTs exhibits an onset potential of 300 mV for generating 1 mA/cm^2 and an overpotential of 393 mV for generating 10 mA/cm^2, whereas Mo_2C on CNTs exhibits an onset potential of 103 mV for generating 1 mA/cm^2 and an overpotential of 176 mV for generating 10 mA/cm^2. This ~220 mV reduction on required overpotential confirms the substantial impact of using Mo_2C over Mo as the functionalization species, with Mo_2C on CNTs surpassing the performance of Mo on CNTs.

Fig. 5b compares the Tafel slopes of all the electrodes. It is widely acknowledged that hydrogen evolution occurs through the following possible steps: an initial discharge step (Volmer reaction) and either a desorption step (Heyrovsky reaction) or a recombination step (Tafel reaction). The Tafel slope is a fundamental property of the catalyst, dictated by the slowest or rate-determining step of the hydrogen evolution reaction (HER). Specifically, the Tafel slope should be 120 mV/dec, 40 mV/dec, and 30 mV/dec when the rate-determining step is the Volmer, Heyrovsky, and Tafel reaction, respectively [47]. The platinum electrode (green graph) exhibits a Tafel slope of 35 mV/dec, serving as the reference, while the Mo_2C on the CNTs sample (red graph) shows a comparable Tafel slope of 95 mV/dec, indicating improved performance due to molybdenum carburization. Conversely, the Mo on CNTs sample (grey graph) shows a Tafel slope value of 105 mV/dec, and pristine CNTs (blue graph) show the poorest performance with a Tafel slope of 150 mV/dec, underscoring the necessity of CNT functionalization for HER purposes. The reduced Tafel slope value of the carburized Mo compound reveals faster reaction kinetics which lead to more efficient hydrogen evolution, via a Volmer–Heyrovsky mechanism.

From the extrapolation of the Tafel slope (Fig. S4 in the supporting information), the exchange current density (Jo) values for different catalysts are obtained, which are summarized in Table 1, Higher Jo values indicate an enhanced electrocatalytic performance towards Hydrogen Evolution Reaction (HER) [48]. Pt (Jo = 8.05 x 10^{-4} mA/cm^2), commonly used as a benchmark, shows the highest exchange current density, indicating its well-known superior catalytic activity.

However, the Mo_2C on CNTs sample that was fabricated in this study exhibits a Jo of 1.36x10^{-4} mA/cm^2, a significant improvement over Mo on CNTs (8.10x10^{-7} mA/cm^2) and CNTs alone (1.08x10^{-4} mA/cm^2). This result highlights the enhanced catalytic performance of Mo_2C on

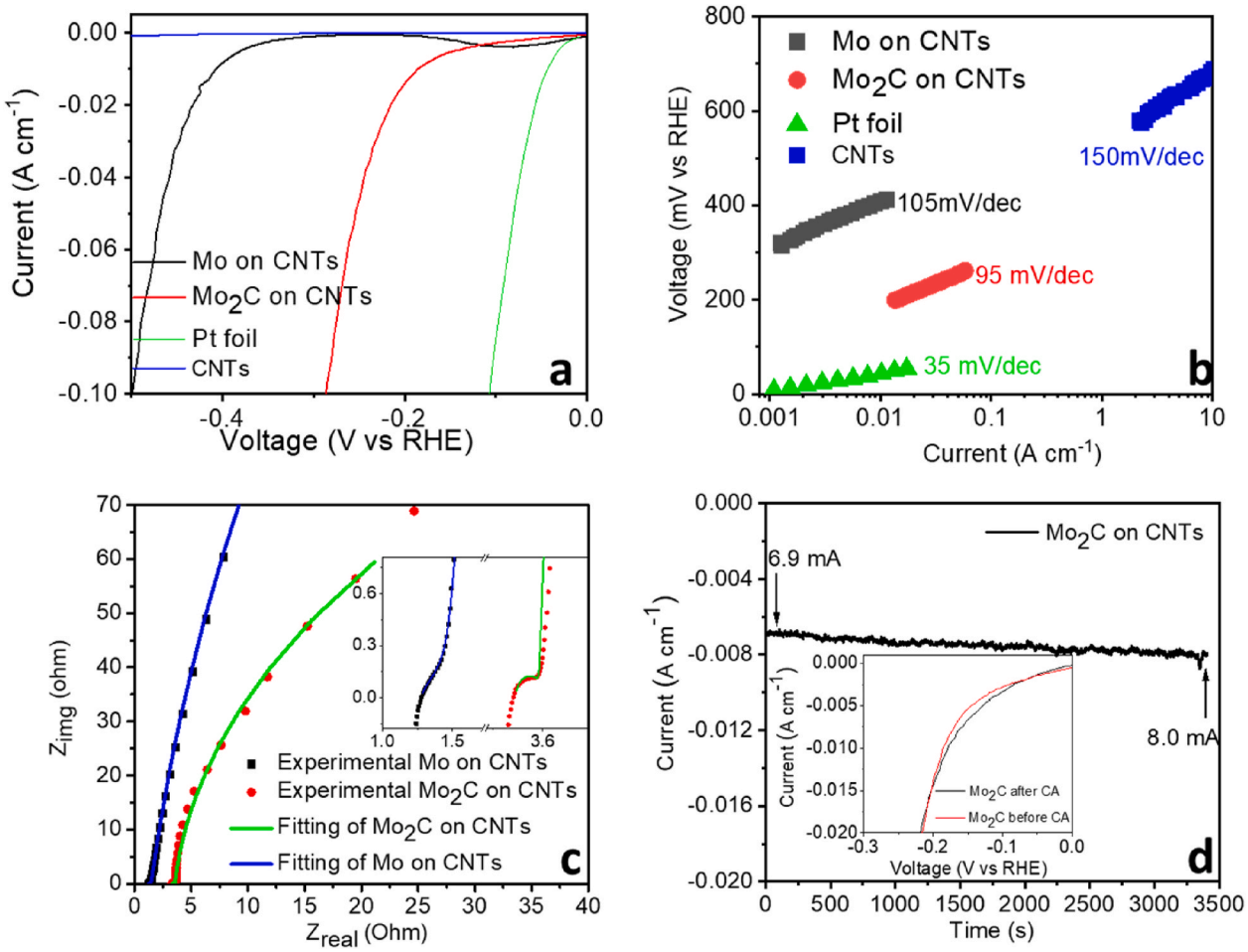

Fig. 5. The electrochemical tests performed a) LSV curves b) Tafel Slopes c) EIS curves, d) Chronoamperometry and a comparison of LSV before and after chronoamperometry (inset).

Table 1
Exchange current densities obtained by extrapolation of Tafel slopes.

Sample	Exchange Current Density (Jo) (mA/cm^2)
Mo_2C on CNTs	$1.36x10^{-4}$
Mo on CNTs	$8.10\ x10^{-7}$
CNTs	$1.08\ x10^{-4}$
Platinum	$8.05\ x10^{-4}$

CNTs due to the synergistic effect between the molybdenum carbide and the carbon nanotubes, which likely facilitates better electron transfer and active site availability.

While platinum remains a stronger catalyst, the much lower cost and relatively competitive performance of Mo_2C on CNTs make it an appealing alternative for HER applications.

Fig. 5c presents a Nyquist plot obtained from EIS, depicting impedance in the system, and providing insight into reaction kinetics and resistance. A smaller semicircle suggests faster charge transfer and a better catalytic performance. Here, the carburized sample displays a smaller semicircle compared to non-carburized molybdenum, favoring Mo_2C on CNTs for HER. The fitting curves are used to extrapolate the series and charge transfer resistances of the equivalent circuit (see Table S1, Fig. S5 and related discussion in supporting information file).

Fig. 5d shows the results of the chronoamperometry test with the Mo_2C on the CNTs electrode. This test assesses reaction speed and electrode stability over time. A constant potential of 0.41 mV was applied to the electrode where it exhibited stability throughout the 3500 s test duration, with performance steadily increasing to 8.0 mA of current generation compared to the initial 6.9 mA. A longer 10hrs chronoamperometry test has been included in the supporting information as Fig. S6 to show the stability of the electrode over a longer period of time. Post-test LSV confirms sustained stability and performance, indicating robust stability of the electrode and the structural integrity of the CNTs adhesion with the carbon fibers and the adhesion between the CNTs and the functionalized species.

We obtained the CV Scans at different scan rates for 4 samples, Mo_2C on CNTs, Mo on CNTs, CNTs on graphite felt and graphite felt. These CV scans can be found in the supporting information Figure S7. From the CV scans (Fig. S7), we obtain the double layer capacitance (C_{dl}) at 0.2 V which is in the non-faraday region. The comparison of the double layer capacitance between the 4 samples are plotted together in the above graph in Fig. 6.

Using this double layer capacitance, we find the electrochemical surface area which is a key parameter for assessing the actual surface available for electrochemical reactions in electrode materials. A high ECSA indicates a large active surface area of the material, which can significantly enhance its energy efficiency. For nanostructured materials such as CNTs and their composites with Mo and Mo_2C, ECSA is particularly important because these materials are designed to maximize the contact surface with the electrolyte, thus increasing capacitance and the rate of electrochemical reactions. The ECSA calculations for four studied materials – Mo_2C on CNTs, Mo on CNTs, CNTs, and graphite felt – show significant differences in the available active surface area, reflecting their unique physicochemical and structural properties. The calculations are supplemented in the supporting information and we can see the

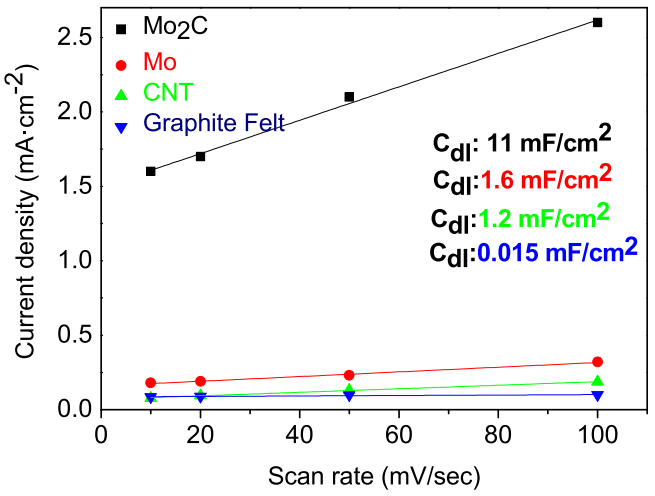

Fig. 6. Double layer capacitance calculations of different samples.

overview of the results in the table below (Table 2).

The highest ECSA value, approximately 314.3 cm^2, was obtained for the Mo_2C on CNTs composite. This high value indicates an exceptionally large electrochemically active surface of this material. The synergistic effect of combining molybdenum carbide (Mo_2C) with carbon nanotubes (CNTs) plays a crucial role. Mo_2C, being a metallic material, provides a large active surface for ion adsorption, which enhances electrochemical capacitance. CNTs, on the other hand, provide a highly porous matrix that allows for efficient ion diffusion and increases the availability of active sites. The combination of these two materials results in a composite with increased electrical conductivity, which minimizes internal resistance and facilitates more efficient charging and discharging processes. The Mo on CNTs material exhibits an ECSA value of 53.3 cm^2, which is significantly lower than that of Mo_2C on CNTs but higher than that of CNTs alone. This suggests that coating CNTs with molybdenum increases their active surface area, though not to the extent achieved with Mo_2C. Mo may not form as stable and dispersed a layer on CNTs, limiting the number of available active sites. Additionally, pure molybdenum has lower electrochemical activity compared to Mo_2C, which may also account for the lower ECSA. Nevertheless, the results show that coating CNTs with metals like molybdenum improves their electrochemical properties. CNTs alone have an ECSA of 20 cm^2. This is relatively low compared to molybdenum-enriched materials. CNTs have high electrical conductivity and excellent mechanical properties, but their active surface area is limited, reducing their ion adsorption capability. For this reason, CNTs are often used as a base for creating more complex composites that can better utilize their unique structural and conductive properties. Graphite felt shows the lowest ECSA value (1.5 cm^2) among the materials studied, due to its less porous structure and limited specific surface area. Graphite has a relatively low active surface area and ion adsorption capability, which limits its effectiveness as an electrode material. Additionally, the lower conductivity of graphite compared to nanostructured carbon materials like CNTs contributes to its lower performance in supercapacitor applications.

In summary, differences in ECSA values among the studied materials are related to their physicochemical properties and structure. Composite materials, such as Mo_2C on CNTs, exhibit the highest ECSA due to the synergy resulting from the combination of different components, which increases the active surface area and improves electrical conductivity.

Table 2
ECSA of 4 samples comparing the large differences in electrochemically active area

Sample	ECSA (cm^2)
Mo_2C on CNTs	314.3
Mo on CNTs	53.3
CNTs	20
Graphite Felt	1.5

The adsorption isotherm for Mo on CNTs takes the shape of type I, characteristic of materials with predominant microporosity [49] (Fig. 7). The rapid increase in the volume of adsorbed nitrogen at low pressures (p/p_o) suggests a large number of micropores, corresponding to a specific surface area of 18.20 m^2/g and a total pore volume of 0.13 cm^3/g. A high specific surface area can enhance catalytic activity in electrochemical reactions by increasing the number of available reactive sites. However, excessive microporosity can lead to pore blockage and hinder the access of reactants and reaction products, potentially reducing the efficiency of the electrochemical process. As a metal, Mo may only partially cover the CNT surface, leaving a significant portion of the carbon nanotubes still accessible. This partial coverage could be advantageous for applications requiring high surface accessibility. However, in terms of stability and effectiveness in electrochemical reactions, partial coverage may not be optimal. In contrast, Mo_2C tends to form a more continuous and compact layer on the CNT surface, which can significantly reduce the accessibility of the CNT's specific surface area. The adsorption isotherm for Mo_2C on CNTs also adopts a type I of isotherm, but the increase in the volume of adsorbed nitrogen at low pressures is less pronounced. The specific surface area of 14.61 m^2/g and the total pore volume of 0.07 cm^3/g are lower compared to Mo on CNTs. The reduced specific surface area and pore volume may result from the filling of micropores by Mo_2C or decreased pore accessibility. The less pronounced hysteresis indicates a more homogeneous porous structure, which promotes better structural stability and minimizes issues related to pore blockage.

The stability and efficiency are crucial in the context of electrochemical hydrogen production. Although Mo on CNTs offers a higher specific surface area, Mo_2C on CNTs can show better efficiency due to its more homogeneous porous structure and stability. Molybdenum carbide, by forming a compact layer, provides better management of reaction products and minimizes issues related to pore blockag.

3.3. Structural characterization post electrochemical analysis

From Fig. 9a we can see the XRD spectrum after electrochemical testing and we see that all the signals related to Mo_2C and graphitic peaks are still present which were present in the XRD spectrum before electrochemical tests presented earlier in the paper in Fig. 8a, confirming that the structural integrity of the electrode is not compromised by the acidic medium of the electrolyte.

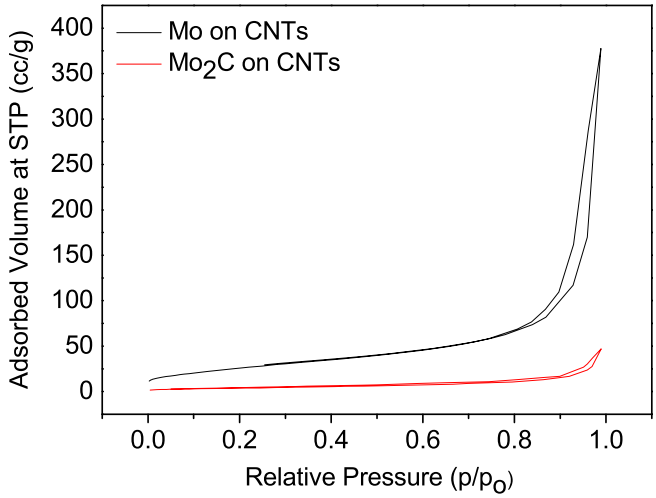

Fig. 7. The BET analysis shows the nitrogen adsorption and desorption isotherms at −196 °C for Mo_2C on CNT and Mo on CNTs.

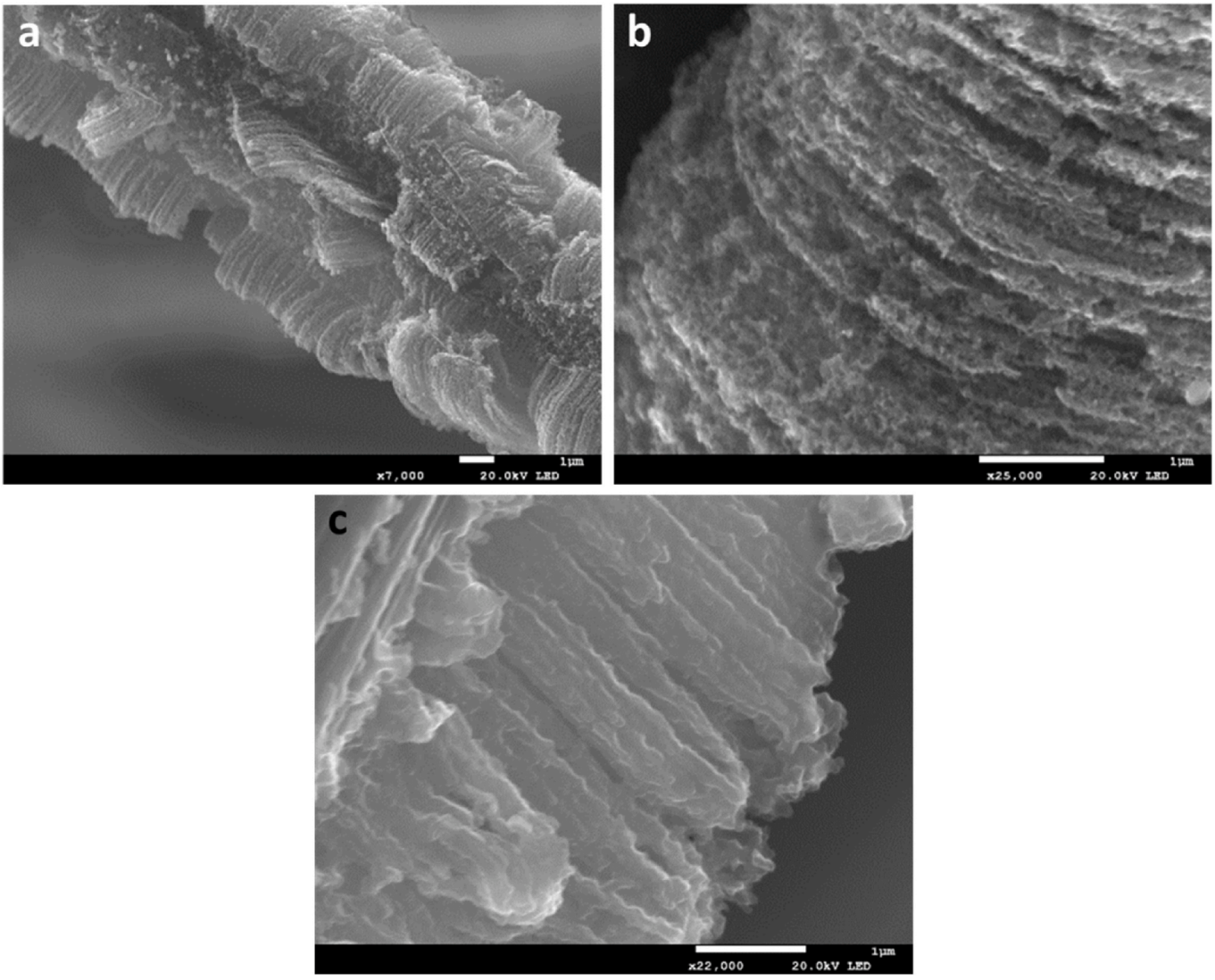

Fig. 8. SEM Images at a)7000x, b) 25000x and c)22000x magnifications taken after electrochemical analysis.

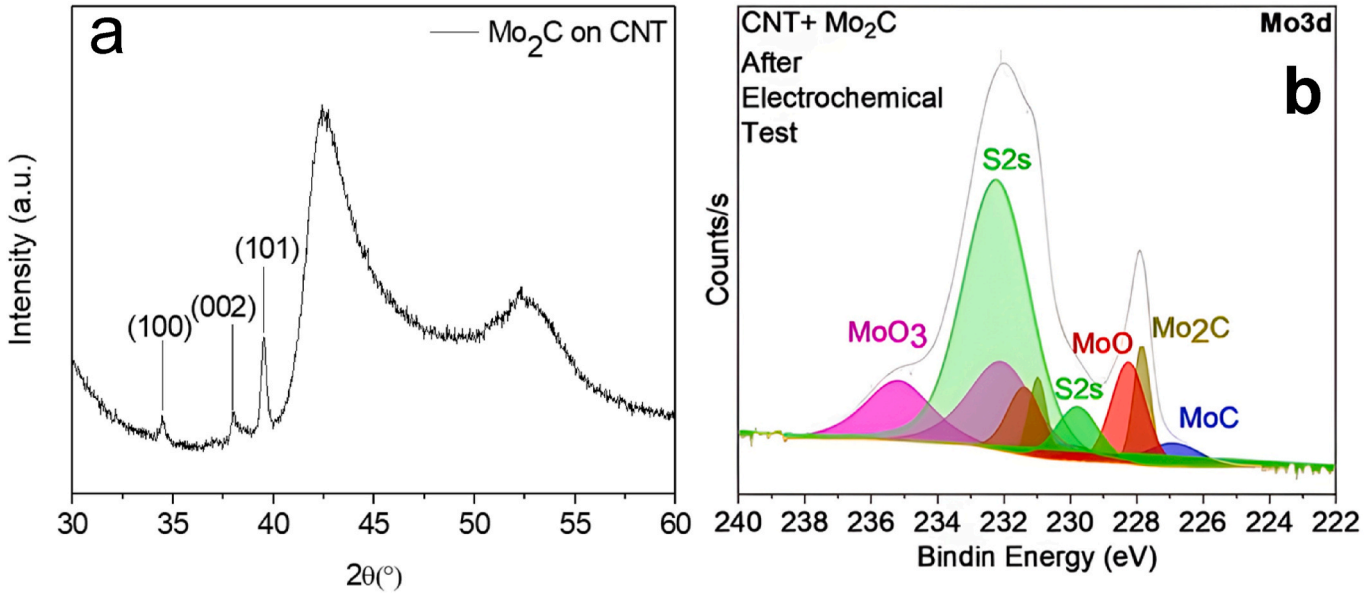

Fig. 9. a) XRD and b) XPS conducted after electrochemical analysis to ensure structural and chemical integrity of the Mo_2C on CNTs hybrid structure.

In the spectra of the Mo_2C on CNTs after the electrochemical test in Fig. 9b we can see the change in the Mo oxidation peaks which occurs as a result of the chemical changes Mo_2C undergoes in the acidic H_2SO_4 electrolyte environment, which causes it to react with S in the electrolyte and produce some S-based compounds like sulphates and S oxides, which change the oxidation peaks. There is also surface oxidation on the Mo_2C and CNT hybrid after being exposed to the electrolyte. Finally, the presence of the Mo_2C peaks at 227.9 eV and 231 eV is confirmed after electrochemical tests thus ensuring the stability of the Mo_2C on the CNTs, despite undergoing some chemical changes during the electrochemical testing.

Additionally, the electrocatalytic performance of various Mo-based catalysts for the HER reaction was evaluated, as shown in Table 3. The primary metrics used for comparison included the overpotential at a current density of 10 mA/cm^2 and the Tafel slope, which indicate catalytic efficiency and reaction kinetics. The results demonstrate that Mo_2C on a novel CNT structure achieves an overpotential of 176 mV and a Tafel slope of 95 mV/dec. This performance is significant, reflecting both low overpotential and favorable kinetics, highlighting the efficiency of this catalyst in HER applications. This work stands out in comparison to other studies, showcasing the potential of Mo_2C functionalization on advanced carbon substrates. For example, Mo_2C on whisker CNTs (WCNTs) shows an even lower overpotential of 164 mV and a Tafel slope of 63 mV/dec, indicating superior reaction kinetics compared to the novel CNT structure. Similarly, Mo_2C in carbon nanocages demonstrates an overpotential of 196 mV and a Tafel slope of 87 mV/dec, which, while competitive, is less efficient than the novel CNT structure. Another noteworthy comparison is with 2D Mo_2C on single-layer graphene, which exhibits a higher overpotential of 236 mV but a lower Tafel slope of 73 mV/dec. This suggests that while it may require higher initial energy input, its reaction kinetics are quite favorable. In contrast, Mo foil, used as a baseline, shows a high overpotential of 399 mV and a Tafel slope of 78 mV/dec, underscoring the enhanced performance of Mo_2C catalysts. Additionally, Mo_2C under single-layer graphene, with an overpotential of 270 mV and a Tafel slope of 56 mV/dec, highlights excellent reaction kinetics but less efficient catalytic activity. Mo_2C in a carbon matrix, displaying an overpotential of 223 mV and a Tafel slope of 78.6 mV/dec, and Mo_2C on graphene nanospheres, with an overpotential of 196 mV and a Tafel slope of 58.6 mV/dec, further illustrate the variability in performance based on the structural context of Mo_2C [39–45]. The synthesis method can determine the interface quality and anchoring of Mo_2C on the C nanostructures, affecting the charge transfer resistance. On the other hand, the C template structure determines the affordable loading of Mo_2C, affecting the electrochemically active surface area and ultimately the electrocatalytic performance [31,50–53].

The novel CNT structure functionalized with Mo_2C demonstrates a compelling balance of low overpotential and moderate Tafel slope, indicating both efficient catalytic activity and favorable kinetics. This comparative analysis underscores the impact of advanced carbon substrates in enhancing the performance of Mo_2C catalysts for HER. The promising results from this study affirm the efficacy of using graphitic felt as an electrode substrate, presenting a cost-effective and energetically efficient solution for hydrogen production.

4. Conclusions

This study successfully demonstrates the deposition of molybdenum on CNTs via magnetron sputtering, with the CNTs grown on a graphite felt substrate's structural and chemical characterization by XPS, XRD and Raman spectroscopy confirms the formation of Mo_2C compounds. The electrochemical performance of the electrode, for HER, is remarkable. Electrochemical tests, including linear sweep voltammetry, electrochemical impedance spectroscopy, and chronoamperometry, show that as-deposited Mo on CNTs exhibits an onset potential of 300 mV to generate 1 mA/cm^2 and an overpotential of 393 mV to generate 10 mA/cm^2. Mo_2C on CNTs shows significant improvement, with an onset potential of 103 mV to generate 1 mA/cm^2 and an overpotential of 176 mV for generating 10 mA/cm^2. Tafel slope analysis reveals values of 150 mV/dec for bare CNTs, 105 mV/dec for Mo on CNTs, and an impressive 95 mV/dec for Mo_2C on CNTs. Although the platinum electrode, with a Tafel slope of 35 mV/dec, is considered the best electrocatalytic material for HER, our Mo_2C on CNT hybrid structure offers comparable performance and serves as an effective and economical alternative.

This work validates the viability of CNTs decorated with Mo_2C as efficient HER electrode material, offering a cost-effective and abundantly available alternative to noble metals like platinum or palladium. Future research on Mo_2C on CNTs could focus on enhancing CNT structures and optimizing the thermal annealing process for in-situ carburization of molybdenum, further improving the material's efficiency and performance.

Table 3
A comparative look at overpotential and Tafel slopes for different Mo based electrocatalysts.

Electrocatalyst used	Overpotential at 10 mA (mV) vs RHE	Tafel slope (mV/dec)	Reference
Mo_2C on dual CNT structure	176	95	**This Work**
Mo_2C on WCNTs (Whisker CNTs)	164	63	[46]
Mo_2C in carbon nanocages	196	87	[54]
Mo_2C on whisker CNTs	187	106	[55]
2D Mo_2C on single layer graphene	236	73	[56]
Mo Foil	399	78	[57]
Mo_2C under single layer graphene	270	56	[57]
Mo_2C in carbon matrix	223	78.6	[58]
Mo_2C on graphene nanospheres	196	58.6	[59,60]

CRediT authorship contribution statement

Shubhadeep Majumdar: Writing – review & editing, Writing – original draft, Methodology, Investigation, Formal analysis, Data curation, Conceptualization. **Stefanos Chaitoglou:** Validation, Supervision, Software, Methodology, Investigation, Formal analysis. **Jarosław Serafin:** Investigation. **Ghulam Farid:** Investigation. **Rogelio Ospina:** Investigation. **Yang Ma:** Investigation. **Roger Amade Rovira:** Project administration, Funding acquisition. **Enric Bertran-Serra:** Project administration, Funding acquisition.

Declaration of competing interest

The authors declare that they have no known competing financial interests or personal relationships that could have appeared to influence the work reported in this paper.

Acknowledgements

The authors acknowledge financial support from Grants PID2020-116612RB-C32, TED2021-132070BC21, and PDC2021-121868-C22 funded by MCIN/AEI/10.13039/501100011033 and by the European Union or by the European Union Next Generation EU/PRTR. The authors acknowledge "Textile Competence Center Vorarlberg 2" (TCCV2 Project FFG 882502) funded within COMET – Competence Centers for Excellent Technologies – by the Federal Ministry for Climate Protection, Environment, Energy, Mobility, Innovation and Technology (BMK) and the Federal Ministry for Digitization and Business Location (BMDW), with co-financing from the federal province of Vorarlberg. The COMET program is managed by the Austrian Research Promotion Agency (FFG).

The ENPHOCAMAT group acknowledges support from the AGAUR of Generalitat de Catalunya, Project No. 2021SGR00936. Y.M. acknowledges the support from the predoctoral fellowship program funded by the China Scholarship Council affiliated with the Ministry of Education of the P. R. China. S.C. acknowledges support from the MSCA postdoctoral fellowship funded by the European Commission through grant agreement 101062014 (HORIZON Europe-MSCA-2021-PF-01). R. O. acknowledges support from the postdoctoral fellowship programme María Zambrano, financed by the European Union and the Spanish Ministry for Science and Innovation. S.M. acknowledges the support from the predoctoral fellowship program funded by TCCV2 Project FFG 882502 within COMET of Austria. The authors also acknowledge CCiT-UB for their help in materials characterization measurements. J.S. is grateful for the financial support provided by the Generalitat de Catalunya through the AGAUR grant for Project No. 2023 CLIMA 00009.

Appendix A. Supplementary data

Supplementary data to this article can be found online at https://doi.org/10.1016/j.ijhydene.2024.09.425.

References

[1] Yue M, Lambert H, Pahon E, Roche R, Jemei S, Hissel D. Hydrogen energy systems: a critical review of technologies, applications, trends and challenges. Renew Sustain Energy Rev 2021;146:111180.
[2] Hu Z, Chen J, Pan P, Liu C, Zeng J, Ou Y, et al. Porous N-doped Mo2C@ C nanoparticles for high-performance hydrogen evolution reaction. Int J Hydrogen Energy 2022;47:4641–52.
[3] Züttel A, Remhof A, Borgschulte A, Friedrichs O. Hydrogen: the future energy carrier. Phil Trans Math Phys Eng Sci 2010;368:3329–42.
[4] Jain I. Hydrogen the fuel for 21st century. Int J Hydrogen Energy 2009;34:7368–78.
[5] Oliveira AM, Beswick RR, Yan Y. A green hydrogen economy for a renewable energy society. Current Opinion in Chemical Engineering 2021;33:100701.
[6] Zhang B, Zheng Y, Ma T, Yang C, Peng Y, Zhou Z, et al. Designing MOF nanoarchitectures for electrochemical water splitting. Adv Mater 2021;33:2006042.
[7] Li X, Hao X, Abudula A, Guan G. Nanostructured catalysts for electrochemical water splitting: current state and prospects. J Mater Chem A 2016;4:11973–2000.
[8] Hwang JY, Kim JY, Youn DH. In-situ construction of Mo2C–MoC heterostructure on Ni foam for efficient hydrogen evolution in alkaline media. Int J Hydrogen Energy 2024;49:58–66.
[9] Cui S, Li M, Bo X. Co/Mo2C composites for efficient hydrogen and oxygen evolution reaction. Int J Hydrogen Energy 2020;45:21221–31.
[10] Zhu Y, Lin Q, Zhong Y, Tahini HA, Shao Z, Wang H. Metal oxide-based materials as an emerging family of hydrogen evolution electrocatalysts. Energy Environ Sci 2020;13:3361–92.
[11] Gao Q, Zhang W, Shi Z, Yang L, Tang Y. Structural design and electronic modulation of transition-metal-carbide electrocatalysts toward efficient hydrogen evolution. Adv Mater 2019;31:1802880.
[12] Hu Y, Guan D-g, Yu B, Hou W, Zheng B, Zhang W, et al. Scalable synthesis of Mo2C/CNT networks as highly efficient and stable electrocatalyst for hydrogen evolution reaction. Electrochim Acta 2018;263:192–200.
[13] Zhang Y, Hu J, Zhang C, Cheung AT, Zhang Y, Liu L, et al. Mo2C embedded on nitrogen-doped carbon toward electrocatalytic nitrogen reduction to ammonia under ambient conditions. Int J Hydrogen Energy 2021;46:13011–9.
[14] Guo T, Zhao R, Chen X, Du Q, Shuai X, Wang Y, et al. Mo-chelate strategy for synthesizing ultrasmall Mo2C nanoparticles embedded in carbon nanosheets for efficient hydrogen evolution. Int J Hydrogen Energy 2021;46:31598–607.
[15] Mir RA, Upadhyay S, Pandey O. A review on recent advances and progress in Mo2C@ C: a suitable and stable electrocatalyst for HER. Int J Hydrogen Energy 2023;48:13044–67.
[16] Chaitoglou S, Ospina R, Ma Y, Amade R, Vendrell X, Rodriguez-Pereira J, et al. Deposition and in-situ formation of nanostructured Mo2C nanoparticles on graphene nanowalls support for efficient electrocatalytic hydrogen evolution. J Alloys Compd 2024;972:172891.
[17] Liu G, Li J, Dong C, Wu L, Liang D, Cao H, et al. Hydrogen evolution reaction on in-plane platinum and palladium dichalcogenides via single-atom doping. Int J Hydrogen Energy 2021;46:18294–304.
[18] Zou X, Tang H, Li J, Gao G, Geng Z, Li L, et al. Phase-controlled synthesis of starch-derived Mo2C–MoC/C heterostructure catalyst for electrocatalytic hydrogen evolution reaction. Int J Hydrogen Energy 2024;79:525–36.
[19] Wang J, Nguyen TH, Dong K, Tran DT, Kim NH, Lee JH. Engineering dual MoC–Mo2C heterostructure–knotted CNTs for efficient direct seawater electrolysis. Int J Hydrogen Energy 2024;49:1005–13.
[20] Cao X, Bai H, Wu W, Bao H, Li Y. Improving the catalytic activity of two-dimensional Mo2C for hydrogen evolution reaction by doping and vacancy defects. Int J Hydrogen Energy 2022;47:38517–23.
[21] Zhang H, Wang L, He W, Liu D, Shao H, Yu W, et al. Mo2C regulated by cobalt components doping in N-doped hollow carbon nanofibers as an efficient electrocatalyst for hydrogen evolution reaction. Int J Hydrogen Energy 2022;47:29337–47.
[22] Hussain S, Vikraman D, Feroze A, Song W, An K-S, Kim H-S, et al. Synthesis of Mo2C and W2C nanoparticle electrocatalysts for the efficient hydrogen evolution reaction in alkali and acid electrolytes. Frontiers in chemistry 2019;7:716.
[23] Huang Y, Bao Y, Huang T, Hu C, Qiu H, Liu H. Carbon nanotube supported molybdenum carbide as robust electrocatalyst for efficient hydrogen evolution reaction. Molecules 2022;28:192.
[24] Chandel A, Kaur G, Upadhyay S, Pandey O. In-situ synthesis of carbon-coated Mo2C: an exceptionally efficient and robust electrocatalyst for hydrogen evolution reaction (HER). Int J Hydrogen Energy 2024;66:512–20.
[25] Šljukić B, Vujković M, Amaral L, Santos D, Rocha R, Sequeira C, et al. Carbon-supported Mo 2 C electrocatalysts for hydrogen evolution reaction. J Mater Chem A 2015;3:15505–12.
[26] Li W, Li X, Zhou W, Dong L, Qin L. Consecutive synthesis of MoO2, Mo2C and MoS2 nanodots as efficient electrochemical hydrogen evolution electrocatalysts. Catal Lett 2024;154:619–26.
[27] Castañeda LF, Walsh FC, Nava JL, de León CP. Graphite felt as a versatile electrode material: properties, reaction environment, performance and applications. Electrochim Acta 2017;258:1115–39.
[28] Coelho NMdA, Furtado JLB, Pham-Huu C, Vieira R. Carbon nanofibers: a versatile catalytic support. Mater Res 2008;11:353–7.
[29] Le TXH, Bechelany M, Cretin M. Carbon felt based-electrodes for energy and environmental applications: a review. Carbon 2017;122:564–91.
[30] Zhang X, Zhu Z, Liang X, Ma F-X, Zhang J, Tan Y, et al. Encapsulating dual-phased Mo2C-WC nanocrystals into ultrathin carbon nanosheet assemblies for efficient electrocatalytic hydrogen evolution. Chem Eng J 2021;408:127270.
[31] Su Y, Chen N, Ren H-l, Li C-w, Guo L-l, Li Z, et al. Application of modified graphite felt as electrode material: a review. Carbon Letters 2023;33:1–16.
[32] Farid G, Amade R, Chaitoglou S, Alshaikh I, Ospina R, Ma Y, et al. Efficient flexible electrodes for lithium-ion batteries utilizing well-dispersed hybrid Mo2C nanoparticles on vertically-oriented graphene nanowalls. J Alloys Compd 2023;968:172109.
[33] Zhang J, Li S, Liu X, Zheng H, Zhang W, Cao R. Co3O4 supported on β-Mo2C with different interfaces for electrocatalytic oxygen evolution reaction. ChemSusChem 2023;16:e202300709.
[34] Li Z, Lu C, Xia Z, Zhou Y, Luo Z. X-ray diffraction patterns of graphite and turbostratic carbon. Carbon 2007;45:1686–95.
[35] Silva VAd, Rezende MC. Effect of the morphology and structure on the microwave absorbing properties of multiwalled carbon nanotube filled epoxy resin nanocomposites. Mater Res 2018;21:e20170977.
[36] Heise H, Kuckuk R, Ojha A, Srivastava A, Srivastava V, Asthana B. Characterisation of carbonaceous materials using Raman spectroscopy: a comparison of carbon nanotube filters, single-and multi-walled nanotubes, graphitised porous carbon and graphite. J Raman Spectrosc: An International Journal for Original Work in all Aspects of Raman Spectroscopy, Including Higher Order Processes, and also Brillouin and Rayleigh Scattering 2009;40:344–53.
[37] Chaitoglou S, Amade R, Ospina R, Bertran-Serra E. Hybrid nanostructured compounds of Mo2C on vertical graphene nanoflakes for a highly efficient hydrogen evolution reaction. ACS Appl Energy Mater 2023;6:6120–31.
[38] Bokobza La, Zhang J. Raman spectroscopic characterization of multiwall carbon nanotubes and of composites. Express Polym Lett 2012;6.
[39] Singh DK, Iyer P, Giri P. Diameter dependence of interwall separation and strain in multiwalled carbon nanotubes probed by X-ray diffraction and Raman scattering studies. Diam Relat Mater 2010;19:1281–8.
[40] Upadhyay S, Pandey O. One-pot synthesis of pure phase molybdenum carbide (Mo2C and MoC) nanoparticles for hydrogen evolution reaction. Int J Hydrogen Energy 2020;45:27114–28.
[41] Brisk MA, Baker A. Shake-up satellites in X-ray photoelectron spectroscopy. J Electron Spectrosc Relat Phenom 1975;7:197–213.
[42] Li Y, Wu X, Liu C, Wang S, Zhou P, Zhou T, et al. Fluorinated multi-walled carbon nanotubes as cathode materials of lithium and sodium primary batteries: effect of graphitization of carbon nanotubes. J Mater Chem A 2019;7:7128–37.
[43] McIntyre N, Johnston D, Coatsworth L, Davidson R, Brown J. X-ray photoelectron spectroscopic studies of thin film oxides of cobalt and molybdenum. Surf Interface Anal 1990;15:265–72.
[44] Jones R, Adams J, Evans S. A new barium molybdate phase. Mater Res Bull 1987;22:351–8.
[45] Kang JS, Kim J, Lee MJ, Son YJ, Chung DY, Park S, et al. Electrochemically synthesized nanoporous molybdenum carbide as a durable electrocatalyst for hydrogen evolution reaction. Adv Sci 2018;5:1700601.
[46] Qiang M, Zhang X, Song H, Pi C, Wang X, Gao B, et al. General synthesis of nanostructured Mo2C electrocatalysts using a carbon template for electrocatalytic applications. Carbon 2022;197:238–45.
[47] Li Y, Wang H, Xie L, Liang Y, Hong G, Dai H. MoS2 nanoparticles grown on graphene: an advanced catalyst for the hydrogen evolution reaction. J Am Chem Soc 2011;133:7296–9.
[48] Chaitoglou S, Giannakopoulou T, Tsoutsou D, Vavouliotis A, Trapalis C, Dimoulas A. Direct versus reverse vertical two-dimensional Mo2C/graphene heterostructures for enhanced hydrogen evolution reaction electrocatalysis. Nanotechnology 2019;30:415404.
[49] Melián-Cabrera I, Mercadal JJ, Mayoral A, Fierro JLG. On the surface area per volumetric loading: its pronounced improvement in densely-packed SWCNT by double-function purification. Microporous Mesoporous Mater 2024;366:112940.

[50] Mondal A, Sinha K, Paul A, Srivastava DN, Panda AB. Large scale synthesis of Mo2C nanoparticle incorporated carbon nanosheet (Mo2C–C) for enhanced hydrogen evolution reaction. Int J Hydrogen Energy 2020;45:18623–34.
[51] Zhan Y, Gao X, Situ A, Huang R, Zhang Z, Pang Z, et al. Sub-2.5 nm monodisperse Mo2C nanoparticles on N-doped carbon: the facet engineering for boosting electrochemical hydrogen evolution. Int J Hydrogen Energy 2024;71. 1326-3.
[52] Chakrabartty S, Raj CR. Mo2C@ NC nanowire bundle for efficient electrocatalytic hydrogen evolution. Int J Hydrogen Energy 2018;43:19510–20.
[53] Elsapagh RM, Sultan NS, Mohamed FA, Fahmy HM. The role of nanocatalysts in green hydrogen production and water splitting. Int J Hydrogen Energy 2024;67:62–82.
[54] Du Q, Zhao R, Guo T, Liu L, Chen X, Zhang J, et al. Highly dispersed Mo2C nanodots in carbon nanocages derived from Mo-based xerogel: efficient electrocatalysts for hydrogen evolution. Small Methods 2021;5:2100334.
[55] Yang C, Shen K, Zhao R, Xiang H, Wu J, Zhong W, et al. Balance effect: a universal strategy for transition metal carbides to enhance hydrogen evolution. Adv Funct Mater 2022;32:2108167.
[56] Geng D, Zhao X, Chen Z, Sun W, Fu W, Chen J, et al. Direct synthesis of large-area 2D Mo2C on in situ grown graphene. Adv Mater 2017;29:1700072.
[57] Chaitoglou S, Giannakopoulou T, Papanastasiou G, Tsoutsou D, Vavouliotis A, Trapalis C, et al. Cu vapor-assisted formation of nanostructured Mo2C electrocatalysts via direct chemical conversion of Mo surface for efficient hydrogen evolution reaction applications. Appl Surf Sci 2020;510:145516.
[58] Wu S, Chen M, Wang W, Zhou J, Tang X, Zhou D, et al. Molybdenum carbide nanoparticles assembling in diverse heteroatoms doped carbon matrix as efficient hydrogen evolution electrocatalysts in acidic and alkaline medium. Carbon 2021;171:385–94.
[59] Yan X, Wang D, Zhang K, Zhang H, Song Y, Liu P, et al. Mo 2 C decorated high-defective graphene nanospheres for improved hydrogen evolution reaction catalytic performance. Catal Lett 2020;150:2141–9.
[60] Ruan Z, Ni J, Yan J, Zhu S, Lu L, Liu Y. β-Mo2C/MoO2 heterostructures for hydrogen evolution reaction: morphology and catalytic activity regulated by heteroatom doping. Int J Hydrogen Energy 2021;46:1517–25.